Applied Physics A (2020) 126:317
https://doi.org/10.1007/s00339-020-03496-4

Applied Physics A
Materials Science & Processing

S.I. : CURRENT STATE-OF-THE-ART IN LASER ABLATION

Numerical simulation of an adaptive beam-shaping technique using a phase grating overlapped via a spatial light modulator for precision square–flat-top beam

Yoshiki Nakata[1] · **Noriaki Miyanaga**[1,2] · **Kazuhito Osawa**[3]

Received: 15 October 2019 / Accepted: 23 March 2020 / Published online: 3 April 2020

Abstract
Beam shape is a key parameter in process optimisation for all laser applications. Among these shapes, a square–flat-top beam is fundamental and is in high demand. To obtain a beam with an aimed structure, various beam-shaping methods have been developed. Among them, an adaptive beam-shaping technique that uses phase grating encoded on a spatial light modulator with spatial frequency filtering in the Fourier plane in a 4*f* system has been developed. In this paper, using precise and simple beam shaping to produce a square and flat-top beam, we examine in detail the phase grating structure via simulations. The directions of the grating vectors inside and outside of the aimed area, i.e. $k_{\text{g-inside}}$ and $k_{\text{g-outside}}$, and the normal vectors of the square and flat-top area, i.e. k_1 and k_2, critically affect the separation of the extracted and residual components on the Fourier plane. To extract the high spatial frequency component for precise shaping, a non-parallel configuration of the grating vectors to the normal vectors of the square beam is found to be effective. This method ensures precision beam shaping as well as keeping of pulse width and wavefront over the shaped area.

Keywords Beam profile · Beam shaping · Spatial light modulator · Phase grating · Flat-top beam

In addition to wavelength, pulse width, power, repetition rate, etc., beam shape is a key parameter in all laser applications. The square–flat-top beam is in great demand for uniform surface processing [1–3], ultra-high power laser facilities [4, 5], skin therapy [6], etc. Considering the high demand, static and adaptive beam-shaping methods have been developed. The former methods, such as microlens array or diffractive diffusers, are simple and cost effective [7]. On the other hand, the edge steepness and flatness produced by these methods are relatively poor. In addition, the wavefront and pulse shape are deformed. In the case of the latter methods, a computer-generated hologram encoded on a spatial light modulator (SLM) imaged by a Fourier transforming lens can generate a far-field arbitrary pattern and has been applied to laser processing [8–10]. However, this approach also has relatively poor performance in terms of pulse shape and wavefront. To overcome these difficulties, adaptive beam-shaping techniques using a phase grating pattern on an SLM with spatial frequency filtering in the Fourier plane in a 4*f* system have been developed (Fig. 1) [11–16]. In this approach, the wavefront is maintained [11]. In addition, beam shaping is drastically improved via the use of a diagonal phase grating [14]. However, the grating structure has not been fully studied.

In this paper, optimisation of the phase grating structure is investigated via simulations. The directions of the grating vectors inside and outside of the aimed area ($k_{\text{g-inside}}$ and $k_{\text{g-outside}}$) and the normal vector of the square and flat-top area (k_1 and k_2) are considered as parameters. In addition, the shape of the spatial frequency filter (SFF), by which the Fourier transformed signal is filtered in the spatial frequency domain, is designed to optimise the resultant beam shape.

✉ Yoshiki Nakata
nakata-y@ile.osaka-u.ac.jp

[1] Institute of Laser Engineering, Osaka University, 2-6 Yamadaoka, Suita, Osaka 565-0871, Japan

[2] Institute for Laser Technology, 1-8-4 Utsubo-honmachi, Nishi-ku, Osaka-city, Osaka 550-0004, Japan

[3] Murata Manufacturing Co., Ltd., 10-1, Higashikotari 1-chome, Nagaokakyo-shi, Kyoto 617-8555, Japan

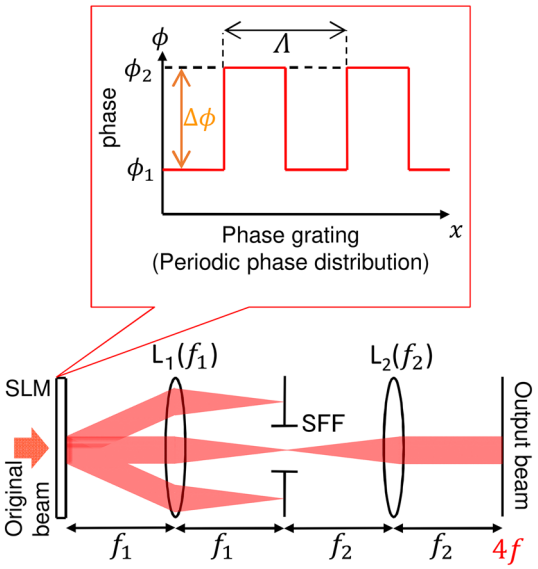

Fig. 1 Scheme of beam shaping. A phase grating is encoded on a spatial light modulator (SLM) and imaged on an output plane at a magnification factor of $M = f_2/f_1$

1 Principle and experimental layout

The scheme is shown in Fig. 1. The phase grating diffracts the residual component, and the extracted component passes only the SFF through the 2D-FFT (two-dimensional fast Fourier transform) via the first convex lens L_1. The component finally forms the desired beam shape via inverse 2D-FFT using the second lens L_2. In this scheme, the electric field intensity at the output plane is expressed by the following equation [14]:

$$E \propto E_0 \cos\left(\frac{\Delta\phi}{2}\right) \times \exp\left(j\frac{\phi_1 + \phi_2}{2}\right) \quad (1)$$

where ϕ_1 and ϕ_2 reflect the phase grating (phase grating depth $\Delta\phi = \phi_1 - \phi_2$). Considering the first cosine term, the intensity can be attenuated by changing $\Delta\phi$. In addition, the exponential term shows that the phase can also be controlled. In another meaning, this approach ensures the keeping of pulse width and wavefront over the shaped area, as discussed in detail later.

The scheme used for beam shaping from an original beam shape to a square–flat-top beam shape via phase grating is shown in Fig. 2. The ratio of the original and desired beam profiles, which are shown in Fig. 2a, b, respectively, is mapped in the transfer function image, as shown in Fig. 2c. Here, $\Delta\phi(x, y)$ can be mapped from the transfer function image using Eq. (1). By encoding $\Delta\phi(x, y)$ to an SLM, beam shaping to a target structure can be achieved.

2 Simulation of the shaped beam from phase gratings

In this investigation, 2D-FFT images are assumed to overlap the phase gratings on a Gaussian beam:

$$E(i,j) = E_0(i,j) \times \exp(k \times \text{grating}(i,j)) \quad (i,j = 1,2,3,\ldots 1024) \quad (2)$$

where $E_0(i,j)$ and $E(i,j)$ express the original and resultant field intensity distribution, respectively, grating(i,j) expresses the phase distribution and k is an imaginary unit. Periods of $\Lambda = 4$ pixels and $\Lambda = 2\sqrt{2} = 2.83$ pixels are assumed for vertical and diagonal phase grating, respectively, as shown in Fig. 3a, b. The pixel size s is assumed to be 20 µm based on the size in a real SLM (Hamamatsu Photonics K.K.). The matrix size corresponds to 20.48 × 20.48 mm in real space, considering to cover the effective area of the SLM and possible SFF filter size. The matrix was transformed by Mathematica © Wolfram. The image was digitised at 8-bit depth of greyscale considering

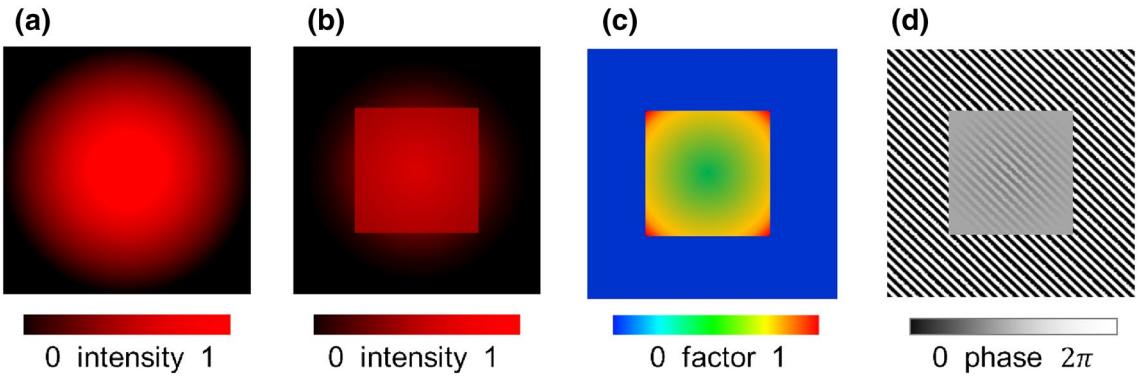

Fig. 2 Scheme for beam shaping to a square and flat-top beam using phase grating: **a** original beam profile, **b** desired beam profile, **c** transfer function image, **d** phase grating image reflecting the transfer function and the output intensity curve as a function of $\Delta\phi$

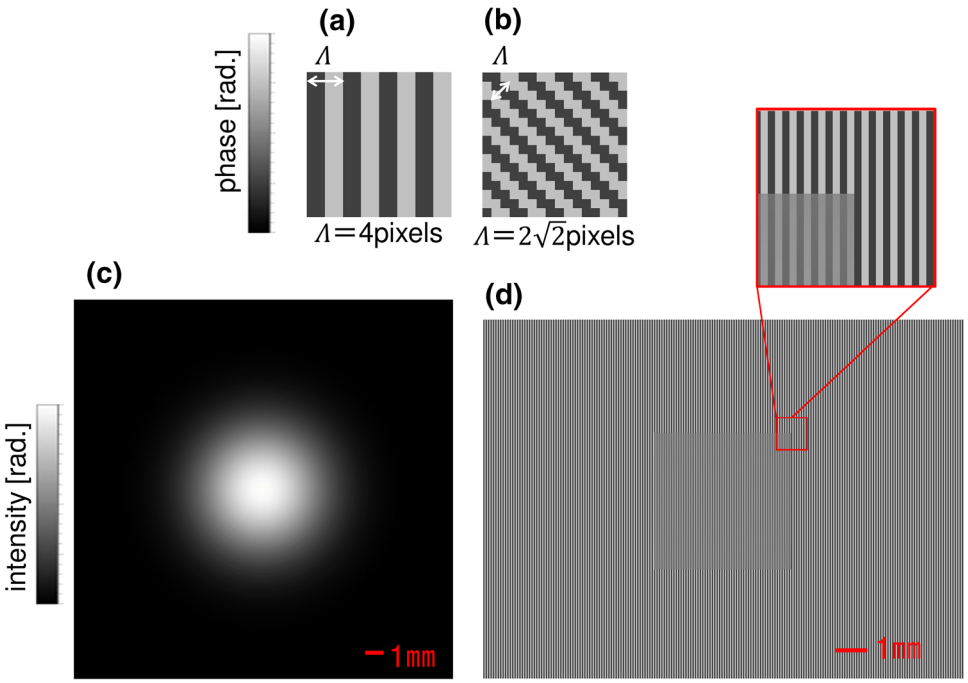

Fig. 3 Models of **a** vertical and **b** diagonal phase grating encoded on an SLM. **c** Gaussian beam with $D = 9.8$ mm diameter, **d** example image of a phase grating image for beam shaping to a square and flat-top beam

the input data format of the SLM. The 2D-FFT transformed data of $E(i, j)$ were transferred to an image by squaring pixel to pixel; they were then filtered by a SFF placed on the Fourier plane. Finally, the image was inverse 2D-FFT transformed. The beam shape and an example of the used phase grating are shown in Fig. 3c, d, respectively. Based on a previous experiment [14], the beam diameter was $D = 9.8$ mm and the focal lengths were $f_1 = 300$ mm and $f_2 = 150$ mm.

3 Beam shape as a function of SFF diameter

Simulated beam shapes as a function of the diameter of the SFF are shown in Fig. 4. Each upper greyscale image shows the 2D-FFT image on the Fourier plane. The area overlapped with grey colour is the SFF area where the beam is blocked. The SFF is co-aligned with the 0th order beam, so a lower frequency component is extracted. Each lower image in the 3D graph shows the resultant beam shape.

When the diameter of SFF $\phi = 1.0$ mm, beam shape is wavy, as shown in Fig. 4a. With a wider SFF, both the ridges on the edge of the square beam and the wavy structure are reduced. Here, concentric circles appearing at the centre of the beam are the result of digital noise. On the other hand, flatness is worsened at $\phi = 6.0$ mm. This is due to the leakage of the residual component from the SFF, which can be seen in the upper image of Fig. 4f. The best result in this condition is produced at $\phi = 5.0$ mm. This is due to regeneration of the beam with the high spatial frequency (HSF) component, which is distant from the centre on the Fourier plane. This is discussed in detail in the next subsection.

4 Relation of the structure of phase grating, desired beam profile and 2D-FFT image

The scheme using vertical phase grating, which is shown in the previous subsection, is highly conventional [11–13]. In this case, the worsening of flatness is due to conflict between HSF component blocking and leakage of the residual component. In this subsection, combinations of the direction of $k_{\text{g-inside}}$ and $k_{\text{g-outside}}$ and normal vectors of the square area, k_1 and k_2, are examined. Moreover, the configuration in which the residual component is blocked while maintaining the HSF component is discussed.

In Fig. 5, different phase gratings and their resultant 2D-FFT images on the Fourier plane are given as a matrix. The upper block shows the case of a square beam where k_1 and k_2 are parallel to the pixel matrix of the SLM. The lower block shows the case of a diamond beam. In the 2D-FFT images, extracted and residual components, as well as their overlap, are shown in red, blue and violet, respectively. To pass the HSF component of the extracted component without leakage of the residual component, overlap must be avoided. From this point of view, the following condition is best:

$$k_{\text{g-inside}}, k_{\text{g-outside}} \nparallel k_1, k_2 \tag{3}$$

Following the condition of Eq. (3), an example of high-quality beam shaping, i.e. with steep edges and flatness, was demonstrated in a previous paper [14].

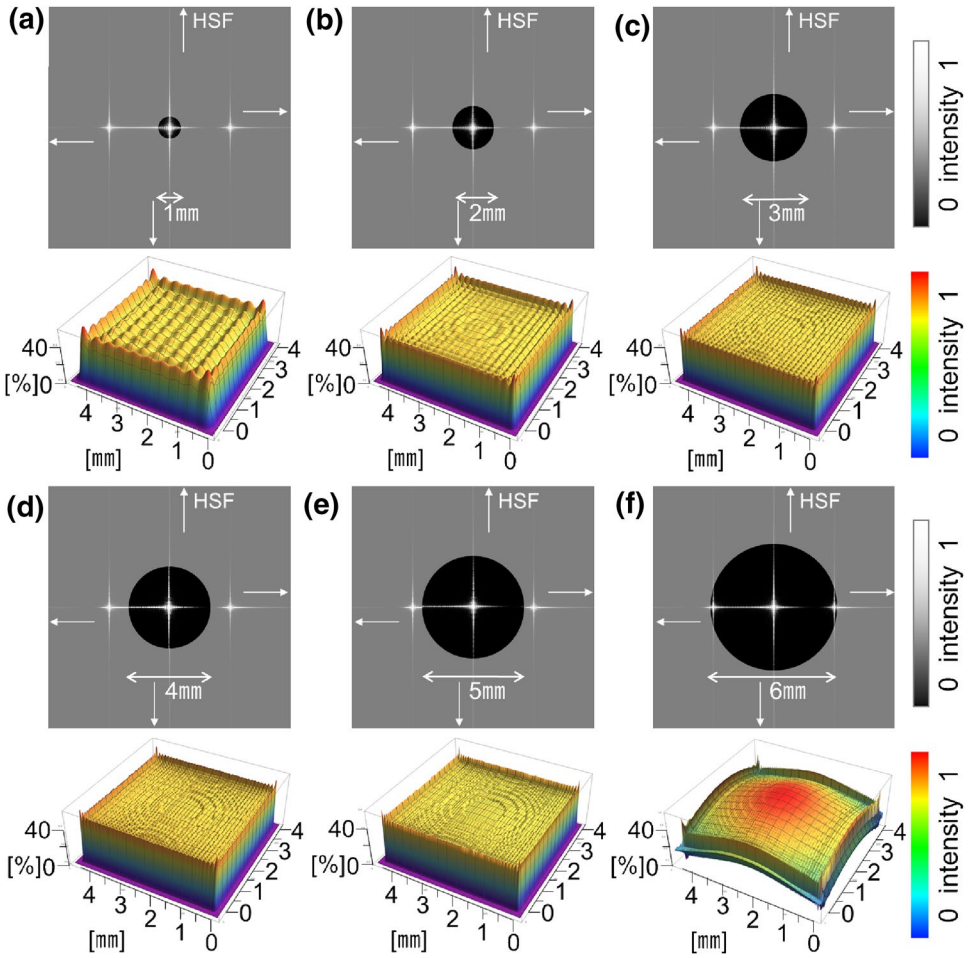

Fig. 4 Simulated beam shape as a function of the diameter of the SFF. The used phase grating is shown in Fig. 3d. A Gaussian beam is aimed to produce a square and flat-top beam with 40 % of the peak intensity

5 Beam shape and efficiency change as a function of SFF shape

In this subsection, the shape of the SFF is changed and the effective extraction of HSF component is examined. Here, circular- and cross-shaped SFFs are tested, as shown in Fig. 6a, b, respectively. The diagonal phase grating is encoded to extract a square beam, as shown in the lower right image in Fig. 5a.

The circular SFF and the resultant beam shape are shown in Fig. 6a. The diameter is $\phi = 2.0$ mm. A wavy structure appears on the beam shape owing to HSF component blocking. The cross-shaped SFF and the resultant beam shape are shown in Fig. 6b. In this case, HSF component can be extracted with complete blocking of the residual component, and the SFF size in real space is 20.48×20.48 mm, which is realistic, as mentioned above. The resultant beam shape is flatter, and ridges on the edges are suppressed. This scheme enables the shaping of super-flat beams with steep edges, as discussed in a previous paper [14].

The efficiency should be compared for those two configurations, and it was 23.07% and 23.31% in Fig. 6a, b, respectively. The difference is small, but the effective extraction of HSF component results in better beam shaping. Here, the efficiency depends on the shape difference between original and shaped beam profiles. Actually, it is not a good combination from Gaussian beam to flat-top square in terms of efficiency. It will be improved by using the combination of Gaussian and flat-top hexagonal, which is under experiment. Moreover, if the original beam shape is similar to the final shape, as in the case of nearly flat-top beam of an excimer laser, the efficiency will be far improved.

6 Pulse width and shape

As known from the exponential term in Eq. (1), the phase is kept over the beam area. This also ensures the keeping of pulse width and shape in the case of the extraction with enough spectral width. For example, consider the case of the Gaussian pulse without chirp. The spectral width is:

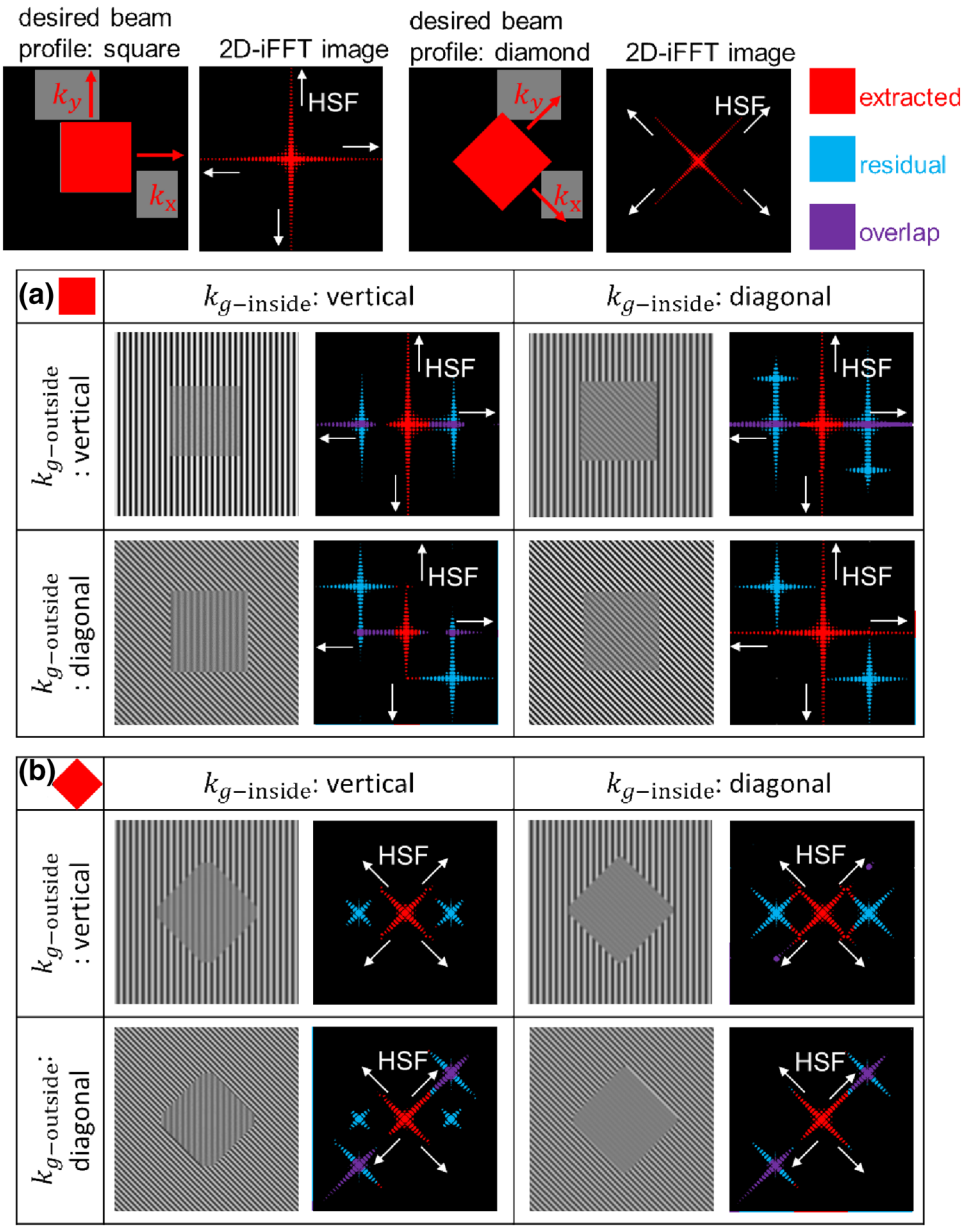

Fig. 5 Combinations of phase grating and the resultant 2D-FFT images appearing on the Fourier plane: **a** square beam and **b** diamond beam to be extracted. The phase grating images are schematic and projected as they appear on the SLM, and the 2D-FFT images are projected as they appear in the Fourier plane from the SLM side. Areas of the extracted component, residual components and their overlap are shown in red, blue and violet, respectively. HFS: high spatial frequency, k_g: grating vector, k_1, k_2: normal vectors

$$\Delta\nu \sim \frac{0.44}{\tau_\mathrm{p}} \tag{4}$$

where τ_p is the pulse width. In the case of 100 fs laser at $\lambda = 800$ nm, the bandwidth $\Delta\lambda = 9.4$ nm. Even though keeping $3\Delta\nu$ to suppress the generation of pedestal and pulse shape change [4], conventional SLM wavelength range covers 3 $\Delta\nu$. Here, beam shaping of a femtosecond laser by using the scheme explained in Fig. 4 has been shown in the past paper [13]. The quality will be improved with keeping the pulse width by using the new scheme introduced in this paper.

7 Summary

We investigated the effect of phase grating structure on the resultant beam shape in an adaptive beam-shaping technique that uses filtering in the spatial frequency domain. To extract HSF component and obtain improved flatness and greater edge steepness, the grating vectors inside and outside the area of a square–flat-top beam must be non-parallel to the normal vectors of the desired beam shape.

The adaptability to the wide wavelength region, of which the capable wavelength of conventional SLM is

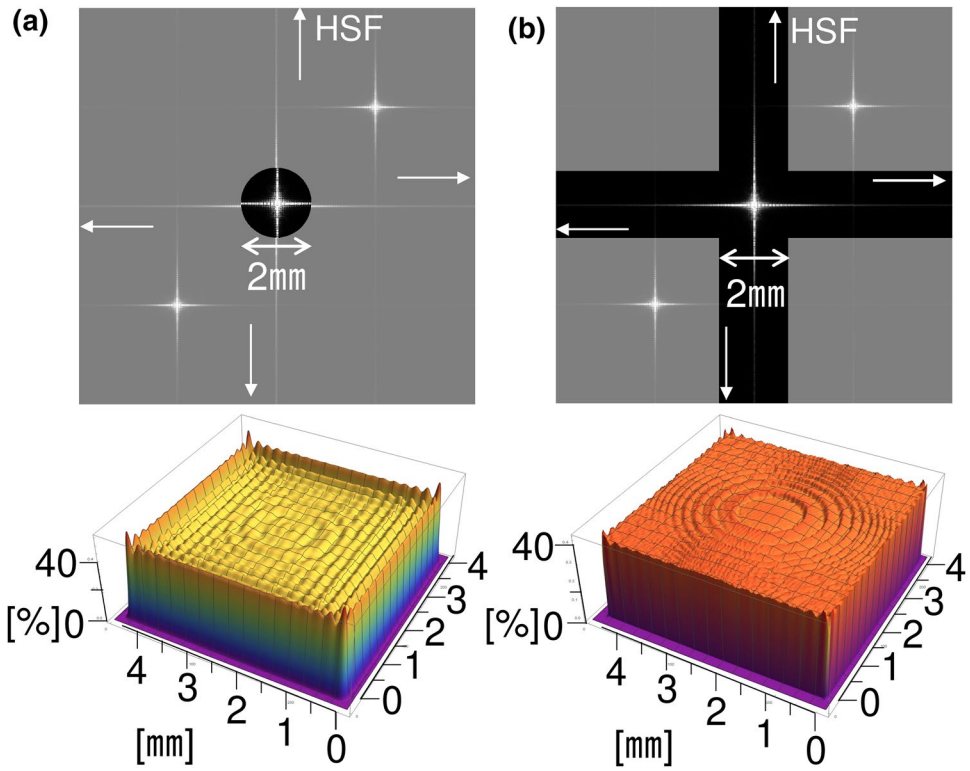

Fig. 6 Simulated beam shape as a function of SFF shape: **a** circular- and **b** cross-shaped SFFs are used. Diagonal phase grating, for which the structure is shown at the lower right of Fig. 5a, is used

approximately 350 nm–1.6 μm, enables optimisation across a variety of applications such as laser annealing, exposure, skin therapy and ultra-high power lasers. In a past experiment, the diagonal configuration of the phase grating relative to the square beam showed system stability as well as quick and easy settings without iterative feedback [14]. Note that the scheme is not restricted to the use of a Gaussian beam as the original beam profile; therefore, its usability is very broad.

From a practical point of view, the SLM is the only cost-consuming component. Compared to the conventional adaptive beam-shaping systems, the performance is far improved by encoding only the diagonal phase grating, without any additional expense. We consider that these advantages will result in the advancement of a variety of laser applications in which beam shape, wavefront, pulse width and shape are critical.

Acknowledgements This research was financially supported by the Japan Society for the Promotion of Science (JSPS) through a Grant-in-Aid for Scientific Research (B) (No. 16H038850) and Amada Foundation.

References

1. Y. Nakata, T. Okada, M. Maeda, Jpn. J. Appl. Phys. Part 2 Lett **42**, L1452 (2003)
2. Y. Nakata, N. Miyanaga, K. Momoo, T. Hiromoto, Appl. Surf. Sci. **274**, 27 (2013)
3. Y. Nakata, T. Hiromoto, N. Miyanaga, Appl. Phys. A Mater. Sci. Process. **101**, 471 (2010)
4. N. Miyanaga, H. Azechi, T. Jitsuno, J. Kawanaka, Y. Fujimoto, H. Shiraga, K. Tsubakimoto, H. Kitamura, H. Matsuo, T. Sakamoto, Y. Izawa, K. Mima, K.A. Tanaka, R. Kodama, K. Kondo, H. Habara, T. Kanabe, J. Phys. IV **23**, 1–8 (2006)
5. S. Sakata, S. Lee, H. Morita, T. Johzaki, H. Sawada, Y. Iwasa, K. Matsuo, K.F.F. Law, A. Yao, M. Hata, A. Sunahara, S. Kojima, Y. Abe, H. Kishimoto, A. Syuhada, T. Shiroto, A. Morace, A. Yogo, N. Iwata, M. Nakai, H. Sakagami, T. Ozaki, K. Yamanoi, T. Norimatsu, Y. Nakata, S. Tokita, N. Miyanaga, J. Kawanaka, H. Shiraga, K. Mima, H. Nishimura, M. Bailly-Grandvaux, J.J. Santos, H. Nagatomo, H. Azechi, R. Kodama, Y. Arikawa, Y. Sentoku, S. Fujioka, Nat. Commun. **9**, 3937 (2018)
6. S. Thomsen, B. Baldwin, E. Chi, J. Ellard, Proc. SPIE **2970**, 287 (1997)
7. P. Dainesi, J. Ihlemann, P. Simon, Appl. Opt. **36**, 7080 (1997)
8. J. Amako, K. Umetsu, H. Nakao, Appl. Opt. **40**, 5643 (2001)
9. N. Sanner, N. Huot, E. Audouard, C. Larat, J.-P. Huignard, B. Loiseaux, Opt. Lett. **30**, 1479 (2005)
10. Y. Hayasaki, T. Sugimoto, A. Takita, N. Nishida, Appl. Phys. Lett. **87**, 20 (2005)
11. V. Bagnoud, J.D. Zuegel, Opt. Lett. **29**, 295 (2004)
12. S.-W. Bahk, E. Fess, B.E. Kruschwitz, J.D. Zuegel, Opt. Express **18**, 9151 (2010)
13. K. Osawa, M. Yoshida, Y. Nakata, N. Miyanaga, A. Narazaki, T. Shoji, Y. Tsuboi, Proc. SPIE **10091**, 100911C (2017)
14. Y. Nakata, K. Osawa, N. Miyanaga, Sci. Rep. **9**, 4640 (2019)
15. Y. Nakata, K. Osawa, Japan Patent application 2018-117035 (2018)
16. Y. Nakata, K. Osawa, International Application No. PCT/JP2019/024533 (2019)